AIP | Conference Proceedings

Are rotating wedges a feasible alternative to dual mirrors for scanning and tracking LDV?

Steve J. Rothberg and Mario Tirabassi

Related Articles

Acousto-microfluidics: Transporting microbubble and microparticle arrays in acoustic traps using surface acoustic waves
J. Appl. Phys. 111, 094911 (2012)

Remote vibration measurement: A wireless passive surface acoustic wave resonator fast probing strategy
Rev. Sci. Instrum. 83, 055001 (2012)

3D mechanical measurements with an atomic force microscope on 1D structures
Rev. Sci. Instrum. 83, 023704 (2012)

Detecting surface acoustic wave gyroscopic signal by acousto-optic coupling
Appl. Phys. Lett. 99, 251116 (2011)

Research on the fiber Bragg grating sensor for the shock stress measurement
Rev. Sci. Instrum. 82, 103109 (2011)

Additional information on AIP Conf. Proc.

Journal Homepage: http://proceedings.aip.org/

Journal Information: http://proceedings.aip.org/about/about_the_proceedings

Top downloads: http://proceedings.aip.org/dbt/most_downloaded.jsp?KEY=APCPCS

Information for Authors: http://proceedings.aip.org/authors/information_for_authors

Are rotating wedges a feasible alternative to dual mirrors for scanning and tracking LDV?

Steve J. Rothberg and Mario Tirabassi

Wolfson School of Mechanical and Manufacturing Engineering,
Loughborough University, Loughborough, Leicestershire, LE11 3TU, UK.

Abstract. An LDV scanning head is proposed based on a pair of rotating optical wedges. Modelling demonstrates how the wedges can be configured to scan point-by-point, in a line and in a circle. The circular scan is considered for the tracking application and shown to offer certain advantages over alternative systems based on dual mirrors and a Dove prism in terms of lower apparent velocities at key rotation orders.

INTRODUCTION

The Laser Vibrometer is now well established as an effective, non-contact alternative to the use of traditional vibration transducers. Special benefits accrue when certain measurement constraints are imposed, for example by the context, which may demand high frequency operation, high spatial resolution or remote transducer operation, or by the structure itself, which may be hot, light or rotating. Among its attractions is the ease with which both the direction of the laser beam and its incident point can be manipulated, as recognised at an early stage with the introduction of the Scanning Laser Doppler Vibrometer (SLDV) [1], scanning point-by-point across a structure with particular applications in the automotive [2-4] and aerospace [5] industries. Today's state-of-the-art offers automated, tri-axial vibration surveys on large, three-dimensional structures (such as a vehicle) using three SLDVs each mounted on a robot arm [6].

In addition to this point-by-point operation, it is possible to configure a SLDV to function in a continuous scanning mode, initially enabling extraction of particular vibration components [7] and ultimately enabling the target velocity profile along a pre-determined path to be determined in a single measurement. In this latter case, post-processing of the measured velocity results in a series of coefficients that describe the operational deflection shape (ODS) or the mode shape [8-13]. If the scan frequency is synchronised with the target motion frequency, it is possible to perform a tracking Laser Vibrometer measurement in which the probe laser beam remains fixed on a particular point on the target [14]. Tracking measurements have been performed on a number of rotor applications [14, 15], as well as on belts (partial track) [16] and on targets with oscillating parts fixed to a component with a large whole body motion such as windscreen wipers [17]. On rotating structures, the attractions of tracking and scanning simultaneously have also been explored [18, 19].

By far the most popular means by which to manipulate the probe laser beam is by using a pair of orthogonally mounted galvanometer mirrors. This approach works well for point-by-point relocation but the inertia of the mirrors, whose accelerations must reach high levels to sustain the required amplitudes of oscillatory motion at high frequency, can limit performance for continuous duty. To overcome this problem in applications such as high speed tracking of rotors, self-tracking systems have been introduced using a combination of a mirror fixed to the rotor itself and a remote mirror that is stationary [20, 21]. This arrangement can be supplemented by scanning (with a traditional dual mirror system) onto the mirror fixed to the rotor to perform scanning while tracking [22]. An alternative rotor tracking system based on a Dove Prism has recently been proposed [23] and is now available commercially [24]. The Dove Prism rotates continuously in the tracking system, rather than in the oscillatory fashion of scanning mirrors, and offers the additional advantage that it need only rotate at half the speed of its target to maintain track.

This paper explores the use of a pair of optical wedges as a scanning head. Like the Dove Prism SLDV, this dual wedge SLDV would overcome the limitation imposed by the inertia of oscillatory mirrors. In a rotor tracking system, the wedges would rotate continuously, only requiring acceleration sufficient to match the structure under

test. The wedges cannot match the additional advantage of the Dove Prism (half speed rotation) but they could offer much of the versatility of the scanning mirrors in terms of point-by–point relocation and the scanning of paths other than circular [25, 26]. Both Dove Prism and wedges require balancing.

Detailed study of proposed new systems and correspondingly detailed comparison with existing systems has been made possible by the recent introduction of a universal framework for predicting measured velocities, beam paths and scan paths in LDV systems, with full geometrical accuracy including routine incorporation of the small but inevitable misalignments to be found in all real systems [27]. The framework also acknowledges the relatively neglected effect of Doppler shifts occurring when laser beam deflection (reflection and refraction) occurs at moving optical devices. The next section sets out how measured and surface velocities are related to each other in general terms. This is then followed by modelling of the dual wedge SLDV within this framework. While focussed on the analysis of a specific system, the model is set out in a manner that is intended to emphasise the generic nature of the modelling framework.

MEASURED VELOCITY AND SURFACE VELOCITY

The fundamental relationship between measured velocity, U_m, and surface velocity at a point P', $\overrightarrow{V_{P'}}$, is captured in the expression [28]:

$$U_m = \frac{1}{2}\left(\hat{b}_{n+1} - \hat{b}_n\right).\overrightarrow{V_{P'}} \tag{1}$$

in which $\hat{b}_{n+1}$ and $\hat{b}_n$ are, respectively, unit vectors for the laser beam directions immediately after and immediately before the point P'. Equation (1) can be applied to incidence at a target surface and to deflections at optical devices. For scattering from the target with light collected in direct backscatter, $\hat{b}_{n+1} = -\hat{b}_n$ and equation (1) simplifies to:

$$U_m = -\hat{b}_n.\overrightarrow{V_{P'}} \tag{2a}$$

With light collected in direct backscatter, deflections at optical devices occur at the same point in both the outgoing and incoming beam path. Based on equation (1), the measured velocity associated with the double pass through a deflection point P' on an optical device is therefore given by:

$$U_m = \frac{1}{2}\left(\hat{b}_{n+1} - \hat{b}_n\right).\overrightarrow{V_{P'}} + \frac{1}{2}\left(-\hat{b}_n - -\hat{b}_{n+1}\right).\overrightarrow{V_{P'}} = \left(\hat{b}_{n+1} - \hat{b}_n\right).\overrightarrow{V_{P'}} \tag{2b}$$

where the unit vector subscripts refer to the outgoing beam path. The total measured velocity is given by the sum of the individual velocities associated with the Doppler shifts at deflections at optical devices and at the target.

Equations (2a&b) highlight the attraction of vector descriptions for surface velocity and beam orientation. This is facilitated by definition of a global xyz coordinate system with origin O fixed in space and unit vectors $\hat{x}$, $\hat{y}$ and $\hat{z}$ associated with its axes. Considering the general case of a rotating and vibrating target, O coincides with a convenient reference point on the target rotation axis in the absence of any vibration. The z-axis is aligned with the target rotation axis, again in the absence of vibration. With vibration, this target reference point moves to O^* as a consequence of its velocity $\overrightarrow{V_{O^*}}$. From fundamental kinematics, surface velocity at the incident point P' is then conveniently written in terms of the sum of the velocity of the reference point and the velocity of P' relative to O^* as a result of rotation at angular velocity $\vec{\omega}$ about an instantaneous rotation axis passing through O^*:

$$\overrightarrow{V_{P'}} = \overrightarrow{V_{O^*}} + \left(\vec{\omega} \times \overrightarrow{r_{P'/O^*}}\right) \tag{3}$$

where $\overrightarrow{r_{P'/O^*}}$ is the position vector for P' relative to O^*. $\vec{\omega}$ includes both continuous target rotation and angular oscillations around the three coordinate axes. For vibrating targets, P' can change continuously and can also be affected by target shape but, for an illuminated target element considered to be rigid, equation (2a) can be expanded in terms of any known point along the line of the laser beam [29], described by the position vector $\overrightarrow{r_0}$:

$$U_m = -\hat{b}_n.\overrightarrow{V_{P'}} = -\hat{b}_n.\left(\overrightarrow{V_{O^*}} + \vec{\omega} \times \left[\overrightarrow{r_0} - \overrightarrow{OO^*}\right]\right) \tag{4a}$$

where $\overrightarrow{OO^*}$ is the target displacement vector associated with the velocity $\overrightarrow{V_{O^*}}$. For applications such as the tracking of a bladed disk, the relative vibration velocity associated with target flexibility must be added to the rigid element velocity [30]. This must be written to accommodate time-dependency in the illuminated point, modifying equation (4a) to become:

6

$$U_m = -\hat{b}_n.\overrightarrow{V_{P'(t)}} = -\hat{b}_n.\left(\overrightarrow{V_{O^*}} + \vec{\omega} \times \left[\vec{r_0} - \overrightarrow{OO^*}\right] + \overrightarrow{V_f(P'(t))}\right) \tag{4b}$$

where $\overrightarrow{V_f(P'(t))}$ is the vector velocity at point $P'(t)$ associated with target flexibility. Later simulations restrict target motions to an in-plane (x) whole body vibration, $V_{O^*x}\hat{x}$, and an out-of plane (z) flexible vibration, $V_{fz}(P'(t))\hat{z}$, combined with target rotation at Ω_T around $\hat{z}$. This represents the important case of a rotating bladed disc attached to a whirling shaft for which the measured velocity, in terms of point T' (where the laser beam intersects the xy plane in which O is located) along the beam, is written:

$$U_m = -\hat{b}_n.\left(V_{O^*x}\hat{x} + \Omega_T\hat{z} \times \left[\overrightarrow{OT'} - \overrightarrow{OO^*}\right] + V_{fz}(P'(t))\hat{z}\right) \tag{4c}$$

In applying the same principles to an optical device, a particular labelling convention is adopted. Without misalignment, a significant point such as a reference point on a rotation axis might be identified as P. With misalignments added, the new position of this point will be labelled P^* and point P may no longer lie on a surface of the optical device. On the surface containing P^*, the point through which the laser beam actually passes will be labelled P' (see Figs. 1a&b). Vectors $\overrightarrow{OP}$, $\overrightarrow{OP^*}$ and $\overrightarrow{OP'}$ define these positions while, for example, the vector $\overrightarrow{P^*P'}$ defines the path from P^* to P'. $\overrightarrow{OP}$ and $\overrightarrow{OP^*}$ will be inputs to the models while $\overrightarrow{OP'}$ and $\overrightarrow{P^*P'}$ will be found as part of the model. Adopting this convention and combining equations (2b) and (3), the measured velocity associated with deflection at an optical device can be written:

$$U_m = \left(\hat{b}_{n+1} - \hat{b}_n\right).\left(\overrightarrow{V_{P^*}} + \vec{\omega} \times \overrightarrow{P^*P'}\right) \tag{5}$$

If P^* is a point on the device rotation axis, $\overrightarrow{V_{P^*}}$ will usually be zero, simplifying equation (5). Exceptions include modelling the effects of vibrations of the device itself.

DUAL WEDGE SLDV

The novel dual wedge SLDV is shown in Fig. 1a. In a system without misalignments, it is possible to define the points A to E. Point A corresponds to the nominal position of the laser source, Points B and C define the rotation axis of the first wedge while points D and E define the rotation axis for the second wedge.
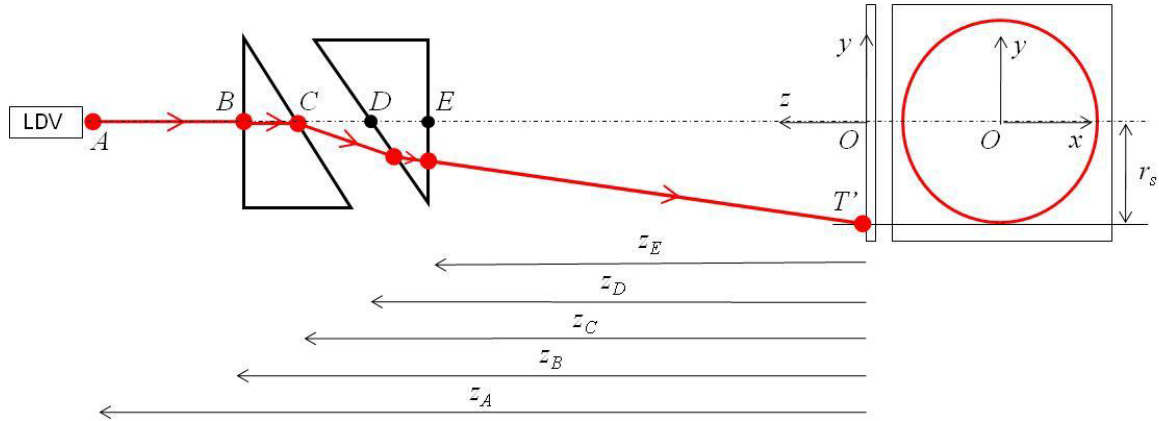

FIGURE 1a. Dual wedge SLDV without misalignments, showing a scanned circle.

Points A and B are written in vector form as:

$$\overrightarrow{OA} = [\hat{x} \quad \hat{y} \quad \hat{z}][0 \quad 0 \quad z_A]^T \tag{6a}$$

$$\overrightarrow{OB} = [\hat{x} \quad \hat{y} \quad \hat{z}][0 \quad 0 \quad z_B]^T \tag{6b}$$

Figure 1b shows the wedges with translational and angular misalignments present, including the points A', B^*, C^*, D^* and E^*. The following equation show how translational misalignments are incorporated into the analysis. The modified vectors $\overrightarrow{OA'}$ and $\overrightarrow{OB^*}$ are written as:
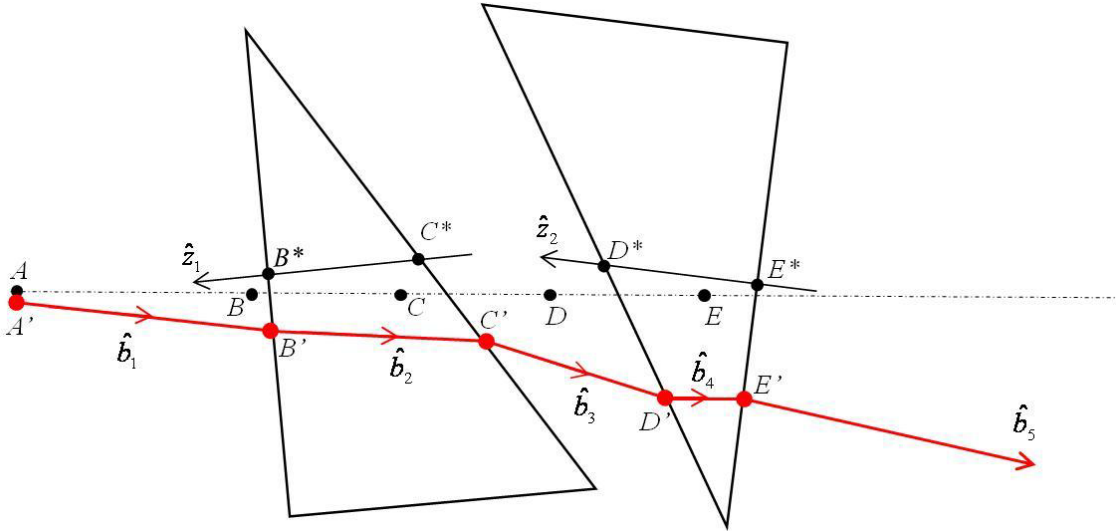
7

$$\overrightarrow{OA'} = \overrightarrow{OA} + [\hat{x} \quad \hat{y} \quad \hat{z}][\Delta x_A \quad \Delta y_A \quad \Delta z_A]^T \tag{7a}$$

$$\overrightarrow{OB^*} = \overrightarrow{OB} + [\hat{x} \quad \hat{y} \quad \hat{z}][\Delta x_B \quad \Delta y_B \quad \Delta z_B]^T \tag{7b}$$

Points D and D* on the second wedge are written in a similar fashion:

$$\overrightarrow{OD} = [\hat{x} \quad \hat{y} \quad \hat{z}][0 \quad 0 \quad z_D]^T \tag{8a}$$

$$\overrightarrow{OD^*} = \overrightarrow{OD} + [\hat{x} \quad \hat{y} \quad \hat{z}][\Delta x_D \quad \Delta y_D \quad \Delta z_D]^T \tag{8b}$$

FIGURE 1b. Misalignment of the wedges and laser head in the Dual Wedge SLDV

Expressions for Points C^* and E^* are defined in terms of B^* and D^*, respectively, and are written in terms of the wedge rotation axes which are themselves affected by angular misalignments. These equations for the wedge rotation axis vectors exemplify the use of rotation matrices (see Appendix A) to modify an initial orientation (in this case $\hat{z}$) to accommodate angular misalignments within the modelling framework:

$$\hat{z}_1 = [\hat{x} \quad \hat{y} \quad \hat{z}][x, \alpha_1][y, \beta_1][0 \quad 0 \quad 1]^T \tag{9a}$$

$$\hat{z}_2 = [\hat{x} \quad \hat{y} \quad \hat{z}][x, \alpha_2][y, \beta_2][0 \quad 0 \quad 1]^T \tag{9b}$$

from which points C^* and E^* are written as:

$$\overrightarrow{OC^*} = \overrightarrow{OB^*} - |\overrightarrow{BC}|\hat{z}_1 \tag{10a}$$

$$\overrightarrow{OE^*} = \overrightarrow{OD^*} - |\overrightarrow{DE}|\hat{z}_2 \tag{10b}$$

The beam path is obviously affected by refractions at each of the four interfaces, requiring knowledge of the corresponding surface normals. These are written in terms of initial alignments modified by a series of rotation matrices. The first rotation matrices are for wedge angle ψ with subscripts '1' and '2' denoting the wedge and subscripts 'a' and 'b' indicating the first or second face of each wedge. The relative orientation of the wedges shown in Figs. 1a&b is arbitrary. The second rotation matrix describes rotations around the z-axis by angles γ_1 and γ_2 for each wedge, respectively, which combine initial angular position with any additional discrete or continuous rotation. Finally, rotation matrices are used to include angular misalignments in the same way as in equations (9a&b).

$$\hat{n}_{B^*} = [\hat{x} \quad \hat{y} \quad \hat{z}][x, \alpha_1][y, \beta_1][z, \gamma_1][x, \psi_{1a}][0 \quad 0 \quad 1]^T \tag{11a}$$

$$\hat{n}_{C^*} = [\hat{x} \quad \hat{y} \quad \hat{z}][x, \alpha_1][y, \beta_1][z, \gamma_1][x, \psi_{1b}][0 \quad 0 \quad 1]^T \tag{11b}$$

$$\hat{n}_{D^*} = [\hat{x} \quad \hat{y} \quad \hat{z}][x, \alpha_2][y, \beta_2][z, \gamma_2][x, \psi_{2a}][0 \quad 0 \quad 1]^T \tag{11c}$$

$$\hat{n}_{E^*} = [\hat{x} \quad \hat{y} \quad \hat{z}][x, \alpha_2][y, \beta_2][z, \gamma_2][x, \psi_{2b}][0 \quad 0 \quad 1]^T \tag{11d}$$

8

Initial beam orientation also makes use of rotation matrices to accommodate angular misalignment and is written

$$\hat{b}_1 = [\hat{x} \quad \hat{y} \quad \hat{z}][x, \alpha_L][y, \beta_L][0 \quad 0 \quad -1]^T \tag{12}$$

Orientations following each refraction are derived using vector expressions [31] that require the vector expressions for each surface normal in equations (11a-d):

$$\hat{b}_2 = \left(\hat{b}_1 - (\hat{b}_1.\hat{n}_{B^*})\hat{n}_{B^*}\right)\frac{\varepsilon_0}{\varepsilon_1} - \left(\sqrt{1 - \left(\frac{\varepsilon_0}{\varepsilon_1}\right)^2 \left(1 - (\hat{b}_1.\hat{n}_{B^*})^2\right)}\right)\hat{n}_{B^*} \tag{13a}$$

$$\hat{b}_3 = \left(\hat{b}_2 - (\hat{b}_2.\hat{n}_{C^*})\hat{n}_{C^*}\right)\frac{\varepsilon_1}{\varepsilon_0} - \left(\sqrt{1 - \left(\frac{\varepsilon_1}{\varepsilon_0}\right)^2 \left(1 - (\hat{b}_2.\hat{n}_{C^*})^2\right)}\right)\hat{n}_{C^*} \tag{13b}$$

$$\hat{b}_4 = \left(\hat{b}_3 - (\hat{b}_3.\hat{n}_{D^*})\hat{n}_{D^*}\right)\frac{\varepsilon_0}{\varepsilon_2} - \left(\sqrt{1 - \left(\frac{\varepsilon_0}{\varepsilon_2}\right)^2 \left(1 - (\hat{b}_3.\hat{n}_{D^*})^2\right)}\right)\hat{n}_{D^*} \tag{13c}$$

$$\hat{b}_5 = \left(\hat{b}_4 - (\hat{b}_4.\hat{n}_{E^*})\hat{n}_{E^*}\right)\frac{\varepsilon_2}{\varepsilon_0} - \left(\sqrt{1 - \left(\frac{\varepsilon_2}{\varepsilon_0}\right)^2 \left(1 - (\hat{b}_4.\hat{n}_{E^*})^2\right)}\right)\hat{n}_{E^*} \tag{13d}$$

Attention is now turned to the identification of deflection points which define beam path and enable derivation of the surface velocities that lead to measured velocity. Key points of incidence are found sequentially beginning from the position of the laser source. A system of three equations is solved; the first is a vector triangle relating the unknown point of incidence to the previous deflection point (or laser source position) through knowledge of beam orientation, the second is a vector triangle relating the unknown point of incidence to a known point on the same optical surface and the third is a dot product between the surface normal and a vector in the plane of the surface. Following this pattern, incidence points B', C', D' and E' (all shown in Fig. 1b) are obtained as follows:

$$\overrightarrow{OB'} = \overrightarrow{OA'} + \left|\overrightarrow{A'B'}\right|\hat{b}_1 \tag{14a}$$

$$\overrightarrow{OB'} = \overrightarrow{OB^*} + \overrightarrow{B^*B'} \tag{14b}$$

$$\overrightarrow{B^*B'}.\hat{n}_{B^*} = 0 \tag{14c}$$

leading to:
$$\overrightarrow{OB'} = \overrightarrow{OA'} + \left[\frac{\left(\overrightarrow{OB^*} - \overrightarrow{OA'}\right).\hat{n}_{B^*}}{\hat{b}_1.\hat{n}_{B^*}}\right]\hat{b}_1 \tag{14d}$$

$$\overrightarrow{OC'} = \overrightarrow{OB'} + \left|\overrightarrow{B'C'}\right|\hat{b}_2 \tag{15a}$$

$$\overrightarrow{OC'} = \overrightarrow{OC^*} + \overrightarrow{C^*C'} \tag{15b}$$

$$\overrightarrow{C^*C'}.\hat{n}_{C^*} = 0 \tag{15c}$$

leading to:
$$\overrightarrow{OC'} = \overrightarrow{OB'} + \left[\frac{\left(\overrightarrow{OC^*} - \overrightarrow{OB'}\right).\hat{n}_{C^*}}{\hat{b}_2.\hat{n}_{C^*}}\right]\hat{b}_2 \tag{15d}$$

$$\overrightarrow{OD'} = \overrightarrow{OC'} + \left|\overrightarrow{C'D'}\right|\hat{b}_3 \tag{16a}$$

$$\overrightarrow{OD'} = \overrightarrow{OD^*} + \overrightarrow{D^*D'} \tag{16b}$$

$$\overrightarrow{D^*D'}.\hat{n}_{D^*} = 0 \tag{16c}$$

leading to:
$$\overrightarrow{OD'} = \overrightarrow{OC'} + \left[\frac{\left(\overrightarrow{OD^*} - \overrightarrow{OC'}\right).\hat{n}_{D^*}}{\hat{b}_3.\hat{n}_{D^*}}\right]\hat{b}_3 \tag{16d}$$

$$\overrightarrow{OE'} = \overrightarrow{OD'} + \left|\overrightarrow{D'E'}\right|\hat{b}_4 \tag{17a}$$

$$\overrightarrow{OE'} = \overrightarrow{OE^*} + \overrightarrow{E^*E'} \tag{17b}$$

$$\overrightarrow{E^*E'}.\hat{n}_{E^*} = 0 \tag{17c}$$

9

leading to:
$$\overrightarrow{OE'} = \overrightarrow{OD'} + \left[\frac{\left(\overrightarrow{OE^*} - \overrightarrow{OD'}\right).\hat{n}_{E^*}}{\hat{b}_4.\hat{n}_{E^*}}\right]\hat{b}_4 \tag{17d}$$

The point T' where the laser beam intersects the *xy* plane is found in similar but slightly simpler fashion

$$\overrightarrow{OT'} = \overrightarrow{OE'} + \left|\overrightarrow{E'T'}\right|\hat{b}_5 \tag{18a}$$

$$\overrightarrow{OT'}.\hat{z} = 0 \tag{18b}$$

leading to:
$$\overrightarrow{OT'} = \overrightarrow{OE'} - \left[\frac{\overrightarrow{OE'}.\hat{z}}{\hat{b}_5.\hat{z}}\right]\hat{b}_5 \tag{18c}$$

Total measured velocity is the sum of the measured velocities from points *B'*, *C'*, *D'*, *E'* and *T'* and is written as:

$$U_m = (\hat{b}_2 - \hat{b}_1).\overrightarrow{V_{B'}} + (\hat{b}_3 - \hat{b}_2).\overrightarrow{V_{C'}} + (\hat{b}_4 - \hat{b}_3).\overrightarrow{V_{D'}} + (\hat{b}_5 - \hat{b}_4).\overrightarrow{V_{E'}} - \hat{b}_3.\overrightarrow{V_{T'}} \tag{19}$$

The surface velocities at the deflection points on each wedge follow the form of equation (5):

$$\overrightarrow{V_{B'}} = \dot{\gamma}_1\hat{z}_1 \times \overrightarrow{B^*B'} \tag{20a}$$

$$\overrightarrow{V_{C'}} = \dot{\gamma}_1\hat{z}_1 \times \overrightarrow{C^*C'} \tag{20b}$$

$$\overrightarrow{V_{D'}} = \dot{\gamma}_2\hat{z}_2 \times \overrightarrow{D^*D'} \tag{20c}$$

$$\overrightarrow{V_{E'}} = \dot{\gamma}_2\hat{z}_2 \times \overrightarrow{E^*E'} \tag{20d}$$

while the relevant component of the target surface velocity is written according to equation (4b).

As presented to this point, the model is totally general. The particular path scanned depends on the functions used for γ_1 and γ_2, and this flexibility delivers the versatility of the proposed dual wedge SLDV.

Point-by-Point and Line Scanning

Fixed values for γ_1 and γ_2 would allow the laser beam to be positioned at a desired location in the target plane for the traditional point-by-point scanning measurement. Individual wedges with deviation angles up to 15° (wedge angle approximately 25°) are available, offering up to a $\pm30°$ field of view.
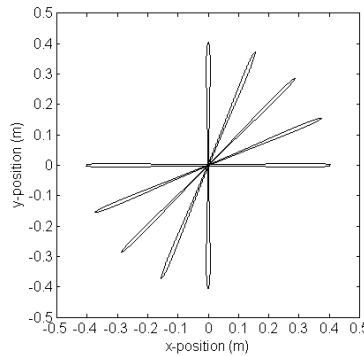

Figure 2. Line scans resulting from wedge rotations at equal speed but opposite direction. (wedge angles 18°, wedge separation 1cm, $z_B = 1.2$m).

A line-scan could be synthesised from the required series of points but a good approximation to a line scan can be created simply through wedge rotation at the equal speed but opposite directions, as shown in Fig. 2. The horizontal orientation results when the wedges have the initial orientation shown in Fig. 1a. Advancing the angular position of wedge 2 in 45° increments up to 180° results in the rotation of the line-scan orientation in increments of half of 45° until the line-scan attains a vertical orientation. Further increments in the initial angular position of wedge 2 result in further rotation of the line-scan orientation. Note that the 'out' and 'back' paths in each line deviate from each other. In this case, the deviation is around 1.25cm or 1.5% of the scan length. Wedge separation and, in particular, wedge angle affect this characteristic of this type of line scan.

10

Tracking

If the intention is to scan a circle, such as might be required to track a point on a target rotating at angular speed Ω_T, then suitable functions are:

$$\gamma_1 = \Omega_T t + \phi_1 \tag{21a}$$

$$\gamma_2 = \Omega_T t + \phi_2 \tag{21b}$$

in which the difference between the initial angular positions of the wedges, ϕ_1 and ϕ_2, determines the scan radius.

In assessing the merits of a newly proposed tracking system, the main areas of interest are any deviations between the desired and actual scan paths and three distinct features of the total measured velocity. These features are the effects of misalignments of the optical system in the presence of target rotation, the sensitivity to target out of plane vibration (the intended measurement), and the sensitivity to target in-plane vibration (an undesired additional measured velocity). The model set out in this paper is well suited to such an evaluation in MATLAB.

In the absence of misalignments, the scan path of the Dual Wedge SLDV is effectively a perfect circle and is very accurately centred on the optical axis. To study misalignments, a very large number of misaligned scenarios have been considered. Resulting scans are checked to ensure that scan radius is within 5% of the intended radius and that the scan centre location is also within 5% of the scan radius from its intended location. Table 1, which compares the performance of the proposed tracking system with those reported previously [27], indicates selection of a much smaller number of configurations for the calculations of measured velocity than the larger number of configurations initially considered as a result of these checks.

a)
b)
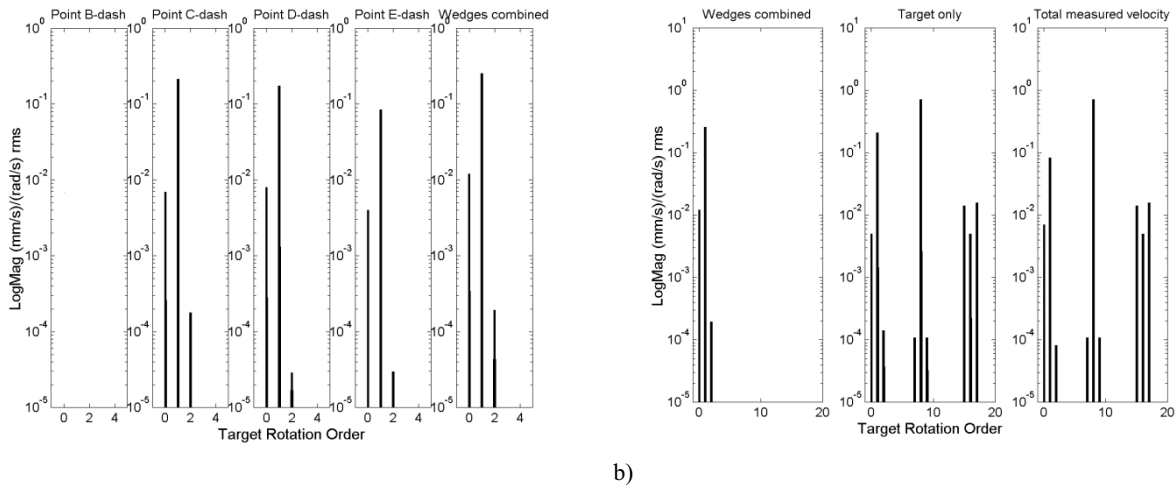
Figure 3. Typical velocities in the Dual Wedge SLDV System in the presence of misalignments ($\alpha_L = 0.1°$, $\beta_L = -0.4°$, $\Delta x_A = -8$mm, $\Delta y_A = -3$mm, $\alpha_1 = -0.1°$, $\beta_1 = 0.4°$, $\Delta x_B = 2$mm, $\Delta y_B = -2$mm, $\Delta z_B = 0$mm, $\alpha_2 = 0.1°$, $\beta_2 = -0.4°$, $\Delta x_D = 2$mm, $\Delta y_D = -2$mm, $\Delta z_D = 0$mm) with 50mm scan radius and sinusoidal target vibrations ($\overrightarrow{V_{fz}}$ of amplitude 10mm/s at $8\Omega_T$ and $\overrightarrow{V_{Ox}}$ of amplitude 10mm/s at $16\Omega_T$):
a) the individual and combined effects of the deflection points on the wedges, and
b) the combined effect of the wedges, the effect of the target and total measured velocity.

In the simulations, vibration frequencies are specifically chosen to allow the effects of misalignment, out-of-plane vibration and in-plane vibration to be distinguished from one another. For the Dual Wedge SLDV in the presence of the typical misalignments listed, Fig. 3a shows velocities associated with the deflections at each wedge deflection point while Fig. 3b shows the combination of velocities from the wedges, from the target and the total measured velocity. These are calculated in accordance with equation (19). With the misalignments chosen, this scan path had a mean radial position of 100.0%, (standard deviation 0.05%) and a centre position error of 3.7%, each relative to the intended 50mm scan radius. Spectral peaks from DC to 2x target rotation order show the effect of misalignments on the total measured velocity. Without misalignments, only DC velocities are associated with Doppler shifts at the second wedge and the target and these cancel completely in the total measured velocity. With misalignments, larger components at DC and 1x, together with a small 2x component appear, as shown in Fig. 3a. Spectral peaks at the same orders are also associated with Doppler shifts at the target, with useful reduction in the

larger components (for this set of misalignments) occurring in the addition of the velocities from the wedges and the target. Consideration of whether Doppler shifts contributing to the total measured velocity originate at optical devices or at the target and of their combination, emphasises the comprehensive detail available in these models.

Across a much greater number of misalignments, Table 1 shows how misalignments affect the low orders in a tracking LDV measurement. In the Dual Wedge system, measurable peaks would be expected at DC and 1x rotation speed. There appear to be advantages over the Dual Mirror and Dove Prism systems in terms of apparent velocity levels and in the absence of the 2x component familiar in Dual Mirror systems and the 0.5x component characteristic of the Dove Prism system. Figure 3b shows an out-of-plane flexible vibration at 8x rotation speed. This characteristic differs little between the three systems considered here with sensitivity of 99.9% with and without misalignment. Misalignments tend to encourage sidebands but they are of very small amplitude and unlikely to be observable in measured data. Figure 3b also shows sensitivity to an in-plane whole body vibration at 16x rotation speed. Without misalignment, there is no peak at the vibration frequency but sensitivity of approximately 2% is found at its $\pm\Omega_T$ sidebands. With misalignments, these sidebands are unaffected but a measurable peak at the in-plane vibration frequency itself now appears for all systems with sensitivity around 0.5%.

TABLE 1. Mean (standard deviation) of rms measured velocities (μm/s / rad/s) associated with system configuration and typical misalignments. 50mm scan radius.

SLDV System	Misaligned configurations used / considered	Order				
		DC	0.5x	1x	1.5x	2x
Dual mirror	No misalignments	No peak	No peak	No peak	No peak	**29.4**
	50621 / 1476225	**5.19 (4.56)**	No peak	**284 (130)**	No peak	**29.4 (2.02)**
Dove prism	No misalignments	No peak	**0.170**	**3.85**	3.01e-2	7.84e-5
	15155 / 540225	**8.72 (7.89)**	**0.219 (4.17e-2)**	**221 (113)**	6.77e-2 (2.87e-2)	4.55e-4 (2.65e-4)
Dual wedges[a]	No misalignments	No peak	No peak	No peak	No peak	No peak
	229635 / 1476225	**6.00 (6.09)**	No peak	**110 (51.7)**	No peak	0.130 (0.0798)

[a] Simulation parameters: $z_A = 1.4$m, $z_B = 1.2$m, $z_D = 1.185$m, $|\overrightarrow{BC}| = |\overrightarrow{DE}| = 5$mm, $\varepsilon_1 = \varepsilon_2 = 1.5$, $\psi_{1a} = 0^O$, $\psi_{1b} = 4^O$, $\psi_{2a} = 4^O$ and $\psi_{2b} = 0^O$. α_L from -0.1^O to 0.1^O in steps of 0.1^O, β_L from -0.4^O to 0.4^O in steps of 0.2^O, Δx_A from -10mm to 10mm in steps of 5mm, Δy_A from -2mm to 2mm in steps of 2mm, α_1 and α_2 from -0.2^O to 0.2^O in steps of 0.2^O, β_1 and β_2 from -1^O to 1^O in steps of 1^O, Δx_B, Δy_B, Δx_D and Δy_D from -3mm to 3mm in steps of 3mm.

CONCLUSIONS

The beam path, scan path and measured velocity associated with a proposed LDV scanning head based on rotating optical wedges have been comprehensively and successfully modelled. Simulations performed suggest that the dual wedge SLDV can be a versatile alternative to the dual mirror SLDV, with advantages including higher frequency operation and lower apparent velocities at key rotation orders.

References

1   B. Stoffregen and A. Felske, Scanning laser Doppler vibration analysis system. *Trans. SAE – Technical Paper Series* 850327 (1985) 934-940. (DOI 10.4271/850327)
2   B. Junge, Experiences with scanning laser vibrometry in automotive industries. *Proc. 1st Int. Conf on Vibration Measurements by Laser Techniques,* (ed. E.P. Tomasini), SPIE vol. 2358 Ancona, Italy, 1994, pp. 377-382.
3   X.D. Zeng, A.L. Wicks and T.E. Allen, Pose estimation of a scanning laser Doppler vibrometer with applications to the automotive industry. *Opt. Eng.* 37(5) (1998) 1442-1447. (DOI 10.1117/1.601653)
4   M.A. Beeck and W. Hentschel, Laser metrology - a diagnostic tool in automotive development processes. *Opt. Lasers Eng.* 34 (2) (2000) 101-120.(DOI 10.1016/S0143-8166(00)00077-4)
5   J. Hancox, B.C. Staples and R.J. Parker, The application of scanning laser Doppler vibrometry in aero-engine development. *Proc. IMechE – J. Aero. Eng.* 209 (1995) 35-42. (DOI 10.1243/PIME_PROC_1995_209_268_02)
6   Polytec, Structure-borne noise measurement with a robot-controlled 3-D scanning laser vibrometer. *InFocus*. 1 (2008) 5-7. http://www.polytec.com/no_cache/int/news/infocus-magazine/?cid=3280&did=3622&sechash=5bca964d (April 2012)

7   A.B. Stanbridge and D.J. Ewins, Measurement of translational and angular vibration using a scanning laser Doppler Vibrometer. *Shock and Vib.* 3(2) (1996) 141-152.

8   P. Sriram, J.I. Craig and S. Hanagud, A scanning laser Doppler vibrometer for modal testing. *Int. J. Analytical and Experimental Modal Analysis* 5(3) (1990) 155-167.

9   A.B. Stanbridge and D.J. Ewins, Modal testing using a scanning laser Doppler vibrometer. *Mech. Syst. Signal Process.* 13(2) (1999) 255-270. (DOI 10.1006/mssp.1998.1209)

10   S. Vanlanduit, P. Guillaume and J. Schoukens, Broadband vibration measurements using a continuously scanning laser vibrometer. *Meas. Sci. Technol.* 13(10) (2002) 1574-1582. (DOI 10.1088/0957-0233/13/10/310)

11   J.P. La, J. Choi, S.Y. Wang, K. Kim and K. Park, Continuous scanning laser Doppler vibrometer for mode shape analysis. *Opt. Eng.* 42(3) (2003) 730-737. (DOI 10.1117/1.1533794)

12   A.B. Stanbridge, M. Martarelli and D.J. Ewins, Measuring area vibration mode shapes with a continuous-scan LDV. *Measurement* 35(2) (2004) 181-189. (DOI 10.1016/j.measurement.2003.07.005)

13   M.S. Allen and M.W. Sracic, A new method for processing impact excited continuous-scan laser Doppler vibrometer measurements. *Mech. Syst. Signal Process.* 24(3) (2010) 721-735. **(**DOI 10.1016/j.ymssp.2009.11.004)

14   P. Castellini, and N. Paone, Development of the tracking laser vibrometer: performance and uncertainty analysis. *Rev. Sci. Instrum.* 71(12) (2000) 4639-4647. (DOI 10.1063/1.1319862)

15   B.J. Halkon and S.J. Rothberg, Vibration measurements using continuous scanning laser vibrometry: advanced aspects in rotor applications. *Mech. Syst. Signal Process.* 20(6) (2006) 1286-1299. (DOI 10.1016/j.ymssp.2005.11.009).

16   P. Castellini and R. Montanini, Automotive components vibration measurements by tracking laser Doppler vibrometry: advances in signal processing. *Meas. Sci. Technol.* 13 (2002) 1266-1279. (DOI 10.1088/0957-0233/13/8/314)

17   H. Dietzhausen, K. Bendel and N. Scelles, Tracking scanning laser Doppler vibrometers: extending laser vibrometry to arbitrarily moving objects. *Proc. IMAC XXI: A Conference & Exposition on Structural Dynamics*, Kissimmee, Florida, 2003, Paper #168 CD-ROM.

18   B.J. Halkon and S.J. Rothberg, Synchronised-scanning laser vibrometry. *Proc.6th Int. Conf. Vibration Measurements by Laser Techniques*, (ed. E.P. Tomasini), SPIE Vol. 5503, Ancona, Italy, 2004 pp 260-271. (DOI 10.1117/12.579759).

19   D. Di Maio and D.J. Ewins, CAISER MYMESIS: a new software platform for virtual and actual vibration testing on rotating structures using a continuously scanning LDV technique. *Proc.7th Int. Conf. Vibration Measurements by Laser Techniques*, (ed. E.P. Tomasini), SPIE Vol 6345, Ancona, Italy, 2006, paper 6345-26 {CD-ROM. (DOI 10.1117/12.693081)

20   R.A. Lomenzo, A.J. Barker and A.L. Wicks, Laser vibrometry system for rotating bladed disks. *Proc. 17th Int. Modal Analysis Conf.* SEM vol. 3727, Kissimmee FL, February 1999 pp. 277-282.

21   I.A. Sever, A.B. Stanbridge and D.J. Ewins, Turbomachinery blade vibration measurements with tracking LDV under rotation. *Proc.7th Int. Conf. Vibration Measurements by Laser Techniques*, (ed. E.P. Tomasini), SPIE Vol 6345, Ancona, Italy, 2006, paper 6345-21. (DOI 10.1117/12.693172)

22   D. Di Maio and D.J. Ewins, Applications of continuous tracking SLDV measurement methods to axially symmetric rotating structures using different excitation methods. *Mech. Syst. Signal Process.* 24(8) (2010) 3013-3036 (DOI 10.1016/j.ymssp.2010.06.012)

23   S. Boedecker, A. Drabenstadt, L. Heller, A. Kraft, A. Leonhardt, C. Pape, S. Ristau, E. Reithmeier and C. Rembe, Optical derotator for scanning vibrometer measurements on rotating objects. *Proc.7th Int. Conf. Vibration Measurements by Laser Techniques*, (ed. E.P. Tomasini), SPIE Vol 6345, Ancona, Italy, 2006, paper 6345-22. (DOI 10.1117/12.693066)

24   Polytec Application Note, "Surface Vibration Measurement on Rotating Components: Non-contact Deflection Shape Analysis on Rotating Components Using the PSV-A-440 Optical Derotator". Available from http://www.polytec.com/eu/products/vibration-sensors/scanning-vibrometers/psv-a-440-optical-derotator/ (April 2012).

25   Rosell, F.A., "Prism Scanner", Journal of the Optical Society of America, 50(6), pp521-526, 1960.

26   Marshall, G.F., "Risley Prism scan patterns", Proceedings of the Conference on Optical Scanning - Design and Application, SPIE Vol. 3787 , pp74-86, 1999, Denver, US.

27   S.J. Rothberg and M. Tirabassi, A universal framework for modelling measured velocity in laser vibrometry with applications. Mech. Syst. Signal Process. 26 (2012) 141-166. (DOI 10.1016/j.ymssp.2011.06.022)

28   B.M. Watrasiewicz and M.J. Rudd, "Laser Doppler measurements", London, Boston, Butterworths, 1976.

29   J.R. Bell and S.J. Rothberg, Laser vibrometers and contacting transducers, target rotation and six degree-of-freedom vibration: what do we really measure? J. Sound Vib. 237(2) (2000) 245-261. (DOI 10.1006/jsvi.2000.3053)

30   B.J. Halkon and S.J. Rothberg, Vibration measurements using continuous scanning laser Doppler vibrometry: theoretical velocity sensitivity analysis with applications. Meas. Sci. Technol. 14 (2003) 382-393. (DOI 10.1088/0957-0233/14/3/318)

31   A.S. Glassner (ed.), An Introduction to Ray Tracing. Academic Press, London, 1989.

Appendix A: Rotation matrices

$$[x, \alpha] = \begin{bmatrix} 1 & 0 & 0 \\ 0 & \cos\alpha & -\sin\alpha \\ 0 & \sin\alpha & \cos\alpha \end{bmatrix} \qquad [y, \beta] = \begin{bmatrix} \cos\beta & 0 & \sin\beta \\ 0 & 1 & 0 \\ -\sin\beta & 0 & \cos\beta \end{bmatrix} \qquad [z, \gamma] = \begin{bmatrix} \cos\gamma & -\sin\gamma & 0 \\ \sin\gamma & \cos\gamma & 0 \\ 0 & 0 & 1 \end{bmatrix}$$

13